Influence of the Electrolyte Quantity on Lithium-Ion Cells

Influence of the Electrolyte Quantity on Lithium-Ion Cells

Florian J. Günter,[z] Clemens Burgstaller, Fabian Konwitschny, and Gunther Reinhart

Technical University of Munich, Institute for Machine Tools and Industrial Management, 85748 Garching, Germany

In the production process chain of lithium-ion battery cells, the filling process is eminent for the final product quality and costs. The filling consists of several dosing steps of electrolyte liquid into the cell and the subsequent (intermediate) wetting of the cell components. The quantity of electrolyte filled not only has an impact on the wetting rate of electrodes and separator but also limits the capacity of the cell and influences the battery lifetime. However, too much electrolyte is dead weight, results in a lower energy density and unnecessarily increases the costs of the battery. To ensure low costs in production and at the same time high quality of the cells, the optimal amount of electrolyte is studied in this paper. Based on experimental data from electrochemical impedance spectroscopy, the filling process, the formation process as well as a lifetime test, the interdependencies between electrolyte quantity, wetting rate, capacity, energy density and lifetime are presented for large-format cells.

 [DOI: 10.1149/2.0121910jes]

Manuscript received March 22, 2019. Published May 29, 2019.

Lithium-ion batteries (LIB) as electrochemical energy storage systems are a key-technology to substitute fossil fuels and enable the storage of renewable resources due to their low weight, high energy densities and long service life.[1] These batteries have established a dominant role in consumer electronics over the last three decades and triggered the success of mobile devices like cell phones and portable computers. Hence, the markets for electric transportation and stationary energy storage are expected to be strongly driven forward by LIB.[2] The goal of higher energy density in automotive applications can be achieved by reducing the percentage of inactive materials, like current collector foils, casing components or separators per cell. This promotes the trend toward larger cell formats[3] as well as thicker electrodes.[4] Large-format cells, however, pose challenges for production processes such as the filling with liquid electrolytes. To ensure reliable operation and high capacity, all cavities and pores of the electrodes and separator have to be wetted before starting the formation cycling.[5] Otherwise, there is the risk of an inhomogeneous solid electrolyte interphase (SEI), which is a reaction product of electrolyte solvent components and lithium on the anode surface.[6] While the SEI on the anode is built during these initial charging and discharging cycles, the cathode electrolyte interphase (CEI) is a result of aging at elevated temperatures or cycling at high voltages.[7] Premature charging prior to the completed wetting can lead to strong local layer thickness fluctuations, which could possibly induce partial layer detachments.[8] Then contrary to the actual function of the SEI, a transfer of electrons from the electrode to the electrolyte (reduction of the electrolyte) and the blocking of ions is possible, which has a negative effect on the capacity and lifetime of the cell.[9]

The increase in number of layers, electrode thickness and surface area per cell decelerates the time consuming wetting of the cell components with electrolyte even further.[10] The small surfaces in coin cells pose no challenge for the wetting, as the electrolyte is able to reach all cavities in a short amount of time. In industrial cell production of large format cells however, multiple periodic wetting and formation cycles are performed resulting in an overall duration of up to 3 weeks.[11] This implies a significant expense, as tens of thousands of cycles as well as storage rooms are needed to manage the required throughput rates.[11]

One way to decrease the costs of LIB is to accelerate the wetting process.[12] Weydanz et al.[13] showed that filling under vacuum down to 100 mbar accelarates this production step significantly. Habedank et al.[14] even achieved 12 times faster wetting by laser structuring of the electrodes, which additionally improves the C-rate behavior.[15] The wetting state is defined as wetted and saturated surfaces and cavities of electrodes and separator compared to the total surfaces and cavities of the cell assembly. The filling of cavities, which are inner surfaces of the media, can be described as microscopic wetting. Whereas the wetting of (macroscopic) surfaces can be regarded as superficial wetting. The former can be measured using electrochemical impedance spectroscopy (EIS).[16,17] The latter can be visualized by neutron radiography.[18] Another way to reduce costs per kilowatt hour is to reduce material costs by minimizing for example the amount of electrolyte per cell.[12] On laboratory scale, disproportionately large quantities of electrolyte are dosed, compared to the surfaces of the components in single-layer cells. In industrial cell production on the contrary, there is not enough empty space in large format-cells to contain electrolyte quantities with the same ratio to the surface of active material and separator.[19] Furthermore, since the electrolyte is inactive material, too much and therefore unnecessary electrolyte is dead weight, which decreases the energy density and increases the costs of the battery.[10]

In order to determine the exact effects of the amount of electrolyte in production, large cells were built and filled with different amounts of electrolyte. These cells were measured during wetting with impedance spectroscopy, then underwent a formation procedure and were cycled in the lifetime test.

Experimental

Cell-Assembly.—The pouch cells, consisting of 13 anode sheets and 12 cathode sheets, were assembled at the Technical University of Munich on semi-automated machines in a dry room with a dew point less than −55°C. The cathode sheets consisted of a double sided coating of $LiNi_{1/3}Co_{1/3}Mn_{1/3}O_2$ (NCM111) on an aluminum collector foil and for the anode graphite was used as active material coated on both sides of a copper collector. The exact specifications of the commercially coated electrodes are shown in Table I. The electrode sheets were separated in a remote laser cutting process as described in Ref. 20 to a format of 101 mm × 73 mm (cathode) and 104 mm × 76 mm (anode). The commercial separator (Celgard 2325) was z-folded between the electrodes to ensure electrical insulation and wrapped around the cell stack for mechanical stability by keeping the electrodes in their exact positions. The tabs and current collector foils were joined using ultrasonic welding and the finished cell stack was

Table I. Specification of the electrodes used.

	unit	cathode	anode
active material	wt%	93.0(NCM111)	92.5(graphit)
conductive carbon	wt%	3.0	0.5
binder	wt%	4.0	7.0
capacity loading	mAh cm^{-2}	2.748	3.606
porosity	%	32.1	32.2
electrode thickness	µm	118	130
substrate foil thickness	µm	20(Al)	10(Cu)

[z]E-mail: florian.guenter@iwb.mw.tum.de

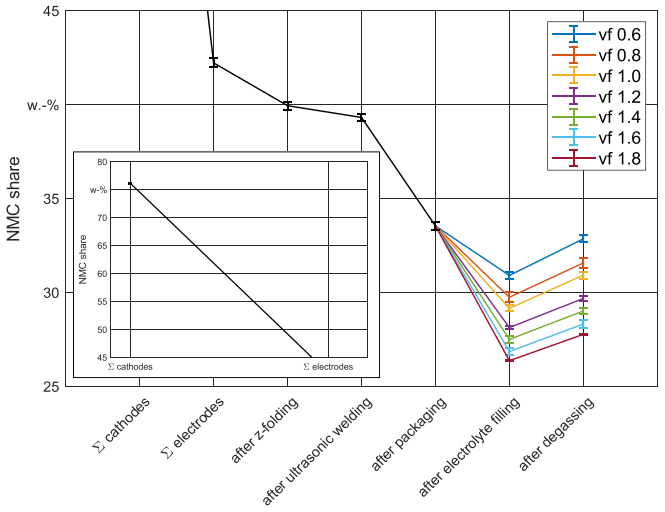

Figure 1. Change of the NMC share over the process steps in the cell assembly after confectioning the electrodes as an indicator for the impact of the cell assembly on the energy density of the product. The volumetric factor vf describes the quantity of electrolyte dosed and is described in Table II.

packaged into the flexible pouch with a deep-drawn pocket. Three sides of the pouch foil were sealed with impulse sealing bars leaving one side open for electrolyte filling. To hinder undesired side reactions with residual humidity as mentioned in Ref. 21, they were dried in a vacuum oven at 60°C and 20 mbar prior to the subsequent filling over night. The details of the filling procedure will be explained in the next section. Before and after each production step, the cells were weighed to map the impact of each process step on the energy density of the product via cell assembly as shown in Figure 1.

Filling-Process.—A 1 M solution of $LiPF_6$ in a mixture of ethylene carbonate (EC) and ethyl methyl carbonate (EMC; weight ratio EC:EMC of 3:7) with 2 wt% vinylene carbonate (VC) from BASF served as electrolyte. Generally, multiple dosing iterations after absorption of the liquid by the cell assembly are required for large-format cells because of the little empty space in the cell and the high flow resistance of the porous structures.[22] For the present experimental design, due to the little electrolyte amount in comparison to the void volume between the flexible pouch foil and the stack, one dosing step was sufficient. As a result, the filling was composed of six steps: flushing with inert gas, evacuation, dosing, sealing, venting and wetting. The electrolyte was dosed in a vacuum chamber at an absolute pressure of 80 mbar. The amount was varied by the volumetric factor

$$vf = \frac{V_{electrolyte}}{V_{pores}} = \frac{V_{electrolyte}}{V_{pores_{Anodes}} + V_{pores_{Separator}} + V_{pores_{Cathodes}}} \quad [1]$$

from 0.6 to 1.8 of the pore volume of the cell components (separator and electrodes). The average pore volume of the cells was 8.85 mL. The dosing accuracy and the resulting electrolyte volumes are summarized in Table II. The closing pressure of the sealing bars was set to 3 bar for 3 seconds with the sealing temperature of 195°C.

After venting the chamber, the cells were kept under ambient pressure for 180 minutes before being charged for the first time. During this wetting, the electrochemical measurements were performed with an Interface 5000E potentiostat from Gamry Instruments. The sequence was composed of open current potential (OCV) and EIS measurements and was programmed to repeat itself for at least 90 minutes. First, the OCV was measured for 15 seconds with a sample period of 0.5 seconds. Subsequently, the potentiostatic EIS was started at an initial frequency of 100 kHz and was changed to 1 Hz with 10 points per decade and an amplitude of 10 rms mV as AC excitation signal applied to the cell. The constant potential offset that can be applied to the cell throughout the data acquisition was set to zero versus the OCV of the cell. The AC voltage was summed with the DC voltage.

The EIS curves were analyzed focusing on the high frequency resistance (HFR). The HFR of the cell is the impedance value at which the imaginary part is zero. It is interpreted as the internal resistance of the cell and changes during the wetting of the cell components with electrolyte liquid.[17]

Formation-Process and lifetime test.—The formation was carried out using a BaSyTec Cell Test System connected to the cells in a temperature chamber at 25°C. The process consisted of 2 cycles at a C-rate of 0.1 C (corresponding to 4.86 Ah_{theor}). The cells were charged in constant current-constant voltage (CCCV) mode with a current limitation corresponding to C/20, while the discharge was done in constant current (CC) mode. The upper cutoff voltage was set to 4.2 V and the lower cutoff voltage was set to 2.5 V.

Before starting the lifetime test, the cells were degassed, removing gas, which was formed during the first charging and discharging cycles through chemical reactions between electrodes and electrolyte as well as the activation of the electrodes. First the cells were measured with EIS using the same routine as in the last section. Due to time steadiness of the EIS, only three measurement cycles were sufficient to capture the impedance behavior of the cell after cycling. Then, the cells were put into the vacuum chamber. The chamber was flushed with inert gas and evacuated to 100 mbar, which was slightly higher than the pressure level for dosing the electrolyte in the last section. The cells were opened to remove the gas and sealed again. After venting the chamber, the superfluous gas bag of the packaging was cut away and the cells were measured again with EIS and weighed.

The reversible capacities of the cells were determined by the second formation cycle. Back in the temperature chamber, the cycling was performed at 1 C (Ah_{rev}) and 25°C in CCCV mode for charging with a current limitation corresponding to C/20 and in CC mode for discharging. Before each set of 50 cylces at 1 C, one cycle at 0.1 C followed by one cycle at at 0.5 C was performed. After completion of the lifetime test, the cells were measured with EIS a fourth time.

For each variation, at least three independent cells were tested and the data in the figures always represents the average of these cells. The error bars in the figures represent the standard deviation of the measurements.

Results and Discussion

Figure 1 shows the mass fraction of the NMC in the total mass of the intermediate product via the processes in the cell assembly. Since (without electrolyte) the active material of the cathode is the only

Table II. Dosing accuracy, resulting amount of dosed electrolyte and capacity of the cells after formation, which correspond to the currents in the lifetime test.

volumetric factor	-	0.6	0.8	1.0	1.2	1.4	1.6	1.8
electrolyte quantity	mL	5.35	7.11	8.77	10.98	12.54	14.26	15.82
standard deviation	mL	0.08	0.04	0.17	0.04	0.13	0.16	0.19
electrolyte quantity	mL Ah^{-1}_{theor}	1.10	1.46	1.81	2.26	2.58	2.93	3.26
cell capacity	Ah_{rev}	2.68	3.23	3.33	3.16	3.28	3.41	3.44
standard deviation	Ah_{rev}	0.12	0.07	0.04	0.07	0.11	0.01	0.02
number of cells	-	3	5	6	3	4	3	4

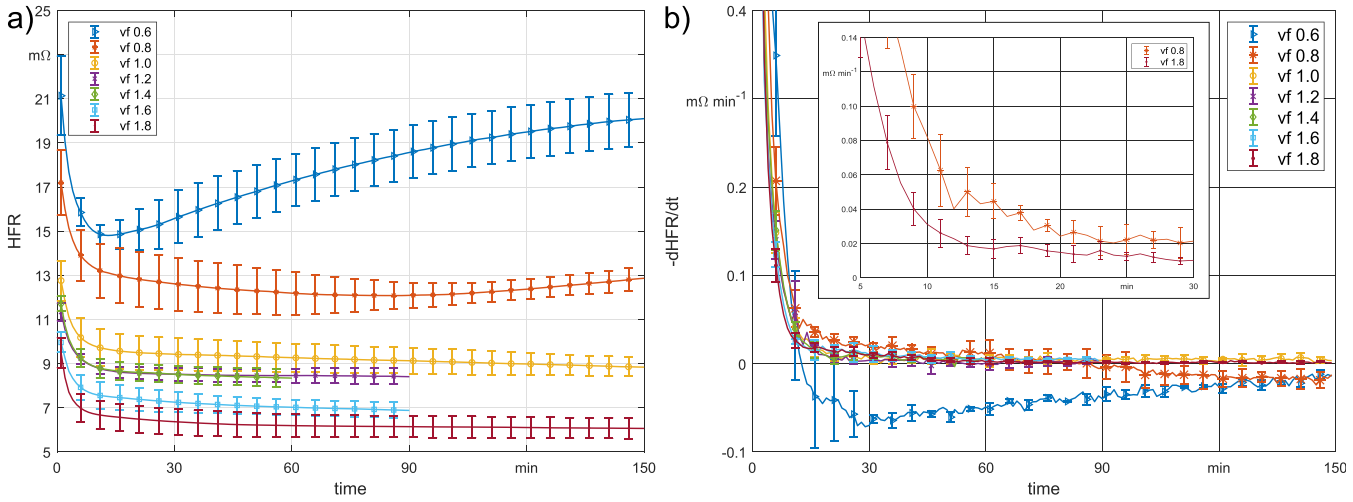

Figure 2. a) HFR of the cells during the wetting with electrolyte liquid; b) Wetting rate as a function of time after dosing of electrolyte liquid.

reservoir of lithium in the cell, the NMC content is an indicator of the energy density of the cell. The initial share of 76% of the cathode is reduced by the assembly steps such as the z-folding, which adds separator and anodes. The weight share is then further increased by the ultrasonically welded-on tabs and the aluminum pouch foil of the packaging. The graph is subdivided into the different electrolyte quantities for the section representing the filling process. With an increase of electrolyte, the weight share of the NMC decreases further. From vf 0.6 to 1.8 a difference of almost 10% in the NMC share is observable. The final increase in the NMC fraction is due to the removal of the waste pouch foil after degassing.

The EIS measurements after dosing of the electrolyte are displayed in Figure 2a for the wetting of the cells. The resulting HFR varies over the time and converges toward a final value as described in Ref. 17. This convergence point is dependent on the amount of electrolyte liquid. Larger dosing quantities result in lower HFR values of the cells after wetting. Furthermore, the HFR decreases and converges for quantities greater than or equal to vf 1, whereas it increases again for smaller amounts before converging. Regarding the wetting rate

$$\dot{\phi} = -\dot{HFR} = -\frac{dHFR}{dt} \qquad [2]$$

(with ϕ as the wetting degree) the effect on the wetting rate also becomes observable in Figure 2b. The wetting rate of cells with vf 0.6 and 0.8 cross the zero line into the negative range and slowly reapproach zero. Unlike cells with larger amounts of electrolyte, these cells have not yet completed wetting within the measurement time of 150 min. The increase in the HFR and the associated longer wetting of the cells is a result of an insufficient amount of electrolyte in the cell. At this point a distinction can be made between two phases of microscopic wetting. During the first wetting phase, the HFR of the cells decreases as in cells with larger electrolyte quantities. The reason for this may be that the electrolyte first penetrates the surface areas of the cell components that are in direct contact with the liquid and begins to compress or replace the residual gas within the pores. This wetting phase ends with the minimum HFR (Figure 2a) or the zero crossing of the wetting speed (Figure 2b). The minimum results from a local oversupply of electrolyte which closes the electric circuit parallel to non-wetted areas during the EIS measurement. In the second phase, the electrolyte liquid is redistributed into the remaining pores, which are not yet filled with electrolyte to the same extent. The capillary forces acting during the intrusion are dependent on the radius of the pores.[23] Therefore, the volume fraction of the electrolyte fluid in small pores increases at the expense of the larger pores with the same contact angle, if not enough electrolyte is present. The second phase is completed when an equilibrium of forces (e.g. capillary forces, gas compression, gravity, etc.) is reached between the pores of all the cell components. Macroscopically, there is now a homogeneous distribution of the electrolyte liquid. The HFR is constant over time and the wetting speed has converged toward zero.

Apart from the undersaturation of electrolyte liquid, detailed mapping of the wetting rate shows that the dependency on the electrolyte quantity is negligible (for the investigated amounts and cell format). The effect of the hydrostatic pressure of the liquid column on the cell stack results in a difference of 0.06 mΩ in the first 10 minutes and declines to less than 0.01 mΩ after 20 minutes. It can be assumed that the hydrostatic pressure has no major impact, since even the maximum dosed volume of 16.01 mL remains small compared to the surfaces to be wetted.

The effects of the electrolyte quantity on the reversible capacity and the energy density of the cells after formation are shown in Figure 3 as a function of the C rate. The volumetric factor 1 corresponds to a metered quantity of electrolyte, which is as large as all cavities of electrodes and separator. However, any interfaces or volumes between the separator and electrodes are not taken into account. In order to achieve the maximum possible capacity by wetting all void volumes, a factor greater than vf 1 is therefore necessary. The capacity at 0.1 C increases from vf 0.6 to 1.2 and then remains constant as vf continues to increase. At 0.5 and 1 C it does not change until vf 1.4. The superior electrical behavior at rates lower than 1 C of the cells with less than or equal to vf 1 can be explained by diffusion of the charge carriers: During these longer charge/discharge phases, the charge carriers have enough time to bypass not (sufficiently) wetted cell areas. The maximum energy density is reached at 0.1 C and vf 0.8. The more electrolyte is dosed into the cells, the lower the energy density becomes after this

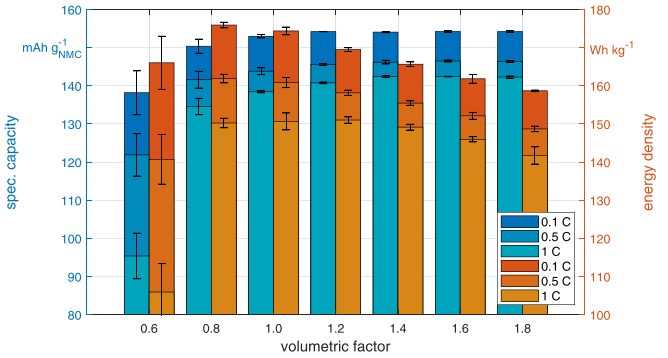

Figure 3. Reversible specific capacity (left bars) and energy density (right bars) of the cells dependent on the electrolyte quantity during the first three cycles (0.1 C, 0.5 C, 1 C) of the lifetime test.

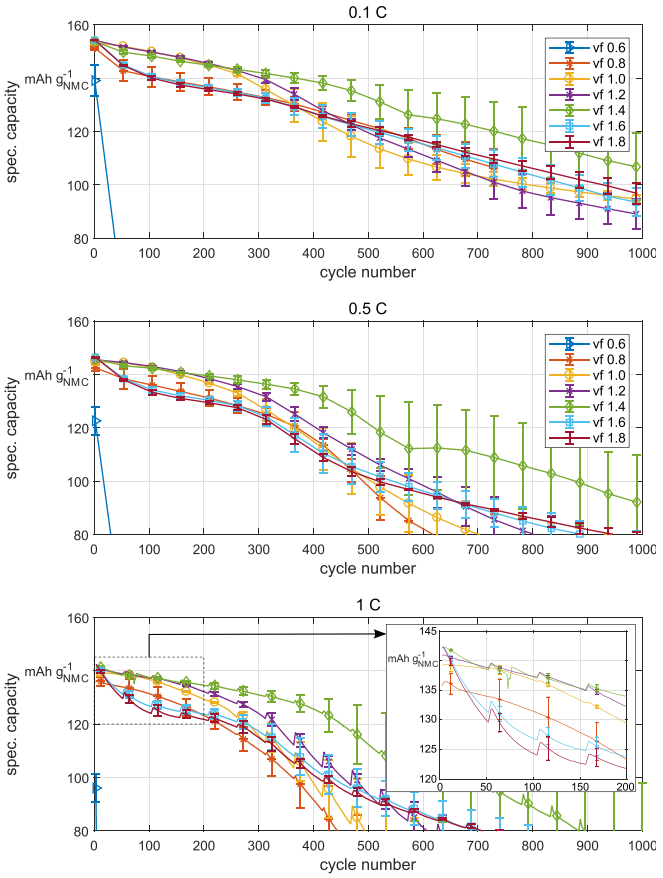

Figure 4. Performance of the cells during the lifetime test after formation. The test was composed of 20·[0.1 C, 0.5 C, 50·[1 C]] cycles in CCCV mode for charging and CC mode for discharging.

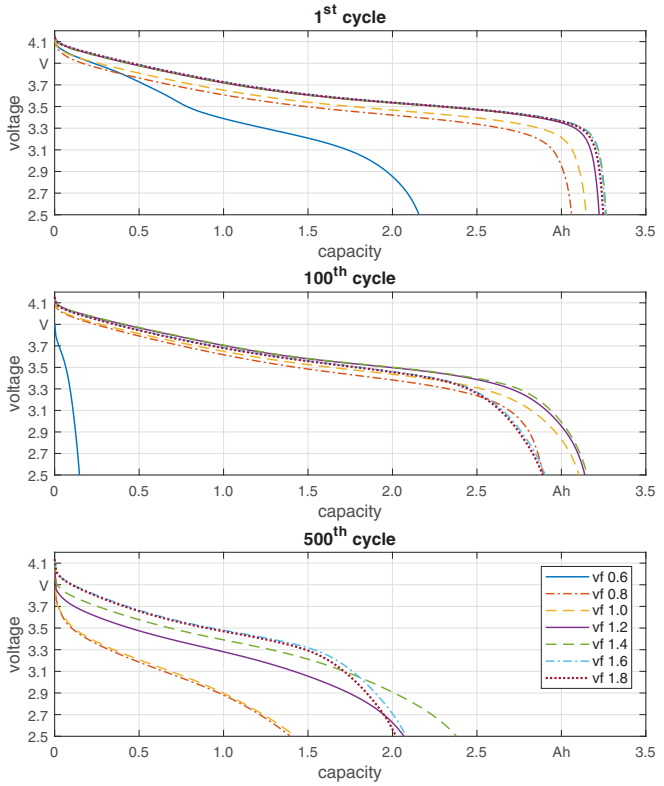

Figure 5. Discharge voltage over the capacity of a characteristic cell as a function of the electrolyte quantity for the 1^{st}, the 100^{th} and the 500^{th} cycle at 1 C of the lifetime test.

peak. The reason for this behavior is the decreasing weight share of the active material, which has a greater influence than the increasing capacity. It can also be shown that the energy density at 1 C does not decrease as quickly as it does at lower C-rates.

Figure 4 displays the specific capacity of the cells during the lifetime test in dependency on the volumetric factor as well as on the C rate. The capacity is higher the lower the C-rate is and decreases with increasing number of cycles. Since the cells are cycled at two lower C-rates after 50 cycles, slight jumps show up in the graph at 1 C, representing the recovery of the cells after low rates. The cells with vf 0.6 already experience a sharp drop in capacity over the first 50 cycles and lose their functionality due to an insufficient amount of electrolyte inside the cells. Yang et al.[24] differentiate between linear and non-linear aging behavior. While SEI growth at the expense of electrolyte plays the dominant role in the linear phase, non-linear aging is an indicator for lithium plating caused by large local electrolyte gradients in the anode and the interface to the separator.[24] Here, after formation, the coulombic efficiency of the cells with vf 0.6[vf 1] is 99%(±1)[102.5%(±1.1)] at 0.1 C. At 1 C it quickly drops to 78%(±2)[95.8%(±0.5)] and then takes about 30 cycles [1 cycle] to reach the efficiency of 97%(±1)[99.9%(±0)]. The capacity, which could not be recovered during discharge indicated by the efficiency, is assumed to be put into a late building of the SEI. In addition to SEI recreation due to cracking during operation,[9] additional SEI is formed by unwetted areas drawing electrolyte from already wetted areas due to a change in the prevailing equilibrium of forces. The low maximum efficieny of 97% at 1 C for vf 0.6 is a result of local poorly or even unwetted areas which have a higher resistance and therefore promote lithium plating in comparison to other areas.[25] With further electrolyte depletion, the ion conductivity through the pores of the separator diminishes ceasing the functionality of the cells. For this reason, the depletion of the electrolyte and the subsequent lithium plating is assumed to be the failure mechanism of the cells.

As the amount of electrolyte increases up to vf 1.4, the performance of the cells improves, so that the loss of capacity over their lifetime is reduced. For larger quantities (vf 1.6-1.8) however, a greater capacity loss can be observed in the enlarged representation of the first 200 cycles at 1 C in Figure 4. The cells can compensate this loss to some extent: Even though the capacity at 0.5 C after 650 cycles is again higher than for vf 1.2 the cells remain below the performance of these with vf 1.4 even at higher cycles. This undesirable effect of the loss of capacity during the first cycles can be attributed to an excess of VC. The additive not consumed during formation builds the CEI during cycling until it is exhausted. Thus it binds lithium, which subsequently can no longer participate in charge exchange.[26]

The two different effects, lithium loss and electrolyte depletion, can also be observed in Figure 5 representing the discharge voltage over the capacity of the cells. During the first cycle, the lack of electrolyte dominates. The more electrolyte is present in the cells, the higher the voltage during discharge and the higher the capacity at which the voltage drops to the cutoff voltage. This is equivalent to a decreasing overpotential with larger electrolyte quantities and thus an increasing discharge capacity of the cell. After 100 cycles, the cell with vf 0.6 has already collapsed. Since high charging rates were applied, at relatively low temperatures, either lithium plating already in the first cycles,[27] or unavailable electrode areas are possible reasons. The cells with vf 1.6 and vf 1.8 remain at higher voltages up to approximately 2.5 Ah, but then drop, so that the capacity of the cells corresponds to that of the cells with vf 0.8. This loss of capacity is attributed to the unavailable amount of lithium which is ligated in the CEI. The cells with vf 1.2 and 1.4 still generate a high voltage over the entire capacity range as well as a high final capacity. However, after 500 cycles these cells (vf 1.2 and 1.4) suffer from a voltage loss in the beginning of the discharge phase, which is supposed to be a result of lithium plating in

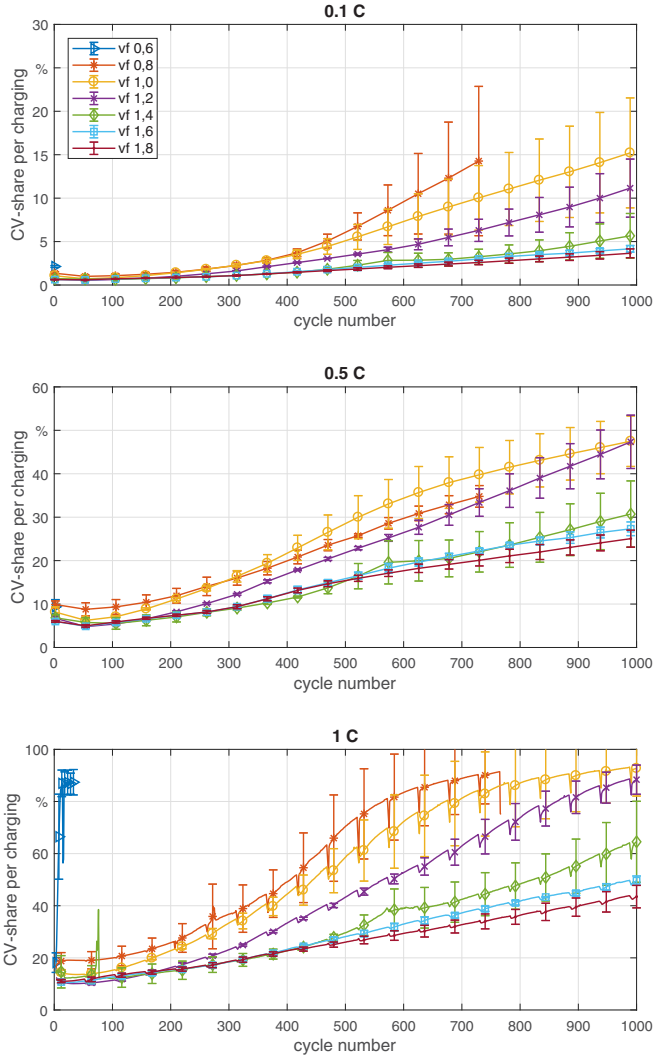

Figure 6. CV-share of the cells during the lifetime test after formation. The CV-share is defined as the capacity charged during CV mode in relation to the total charged capacity during CC and CV mode. The lifetime test was composed of 20·[0.1 C, 0.5 C, 50·[1 C]] cycles in CCCV mode for charging and CC mode for discharging.

combination with an increased SEI. Although cells filled with vf 1.4 still reach the highest capacity, the voltage of vf 1.6 and 1.8 is higher at concurrent lower capacities. In general, the voltage at the beginning of the discharge process seems to drop for less electrolyte being present in the cells. The loss of lithium of the cells (due to an excessive CEI building), however, is indicated by a premature voltage drop from a high level in comparison to cells without excessive CEI.

The CV-share is defined as the capacity charged during CV mode in relation to the total charged capacity Q during CC and CV mode:

$$\frac{Q_{CV}}{Q} = \frac{Q_{CV}}{Q_{CV} + Q_{CC}} \qquad [3]$$

and is shown in Figure 6. The charge percentage can serve as an indicator for the fast-charging capability of the cells and is dependent on the C-rate: With increasing SOC the potential of the cathode increases and the potential of graphite approaches 0 V versus Li^+/Li. The difference between the two potentials determines the cell voltage. Thus, in CC mode, the charging voltage rises to provide the determined current. The anode must intercalate the lithium atoms in a given time (defined by the C-rate). If the intercalation rate at the anode is slower than the transport rate of Li^+ in the electrolyte imposed by the charge current, lithium accumulates at surface of the anode. The potential of

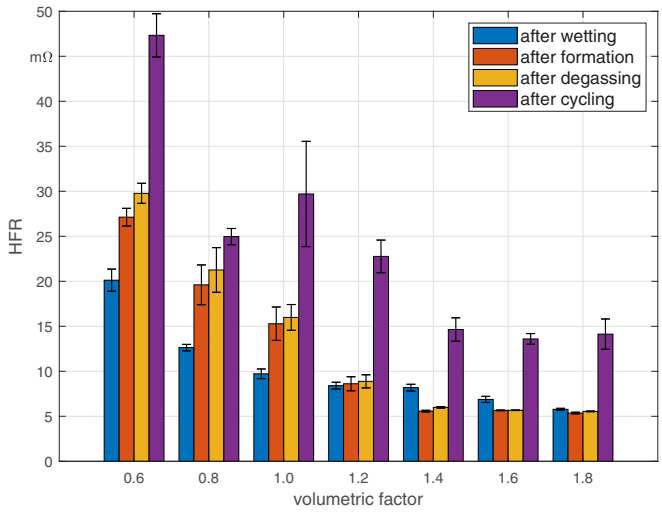

Figure 7. HFR of the cells after wetting, formation, degassing and the lifetime test (1040 cycles without formation) for different electrolyte quantities at SOC 0.

the graphite falls below 0 V versus Li^+/Li and metallic lithium plating occurs on top of the anode. Therefore, high C-rates favor lithium plating.[28] In addition, plating can be induced by non-wetted areas of the anode or the separator through the resulting inhomogeneous distributions of the current density.[29] The negative anode potential (versus lithium) results in a cell voltage over the cathode potential so that the upper cutoff voltage and thus the CV phase is reached earlier.[30] At the upper cutoff voltage level, the voltage is kept constant in CV mode and the cell will be charged until the current drops to the cutoff condition. A small CV-share is therefore synonymous with a high intercalation rate capability of the anode and a fully wetted separator as shown in Figure 6: The more electrolyte is dosed into the cells, the lower the CV-share. With increasing number of cycles and C-rate, the CV-share increases. Therefore, not only must the cells be charged for a longer time, but they are also exposed to higher voltages for a longer time, which represents a strain on the cell components.[31]

The HFR of all cells after wetting, formation, degassing and the lifetime test is displayed in Figure 7. The SOC of all cells was assumed to be 0% as they were either never charged (just wetted) or discharged to a voltage of 2.5 V. The HFR after degassing is slightly higher than after formation. A reason for this could be that a small amount of the electrolyte liquid is drawn out of the pores during degassing and has to reoccupy this space. For the cells with vf 0.6 to 1.2 both HFR values after formation and degassing are higher than the HFR after wetting. From vf 1.4 to 1.8, the HFR after formation and after degassing is lower than after wetting. In combination with the electrochemical performance during the lifetime test, the measurements show that an electrolyte quantity of at least vf 1.4 is required to allow the SEI to form completely during formation and to ensure the optimal ionic conductivity through the separator necessary for charge exchange. The charge transfer between electrolyte and anode is even improved by the formation of SEI with a sufficient amount of electrolyte, as shown by the HFR values. Over the lifetime, however, the internal resistance of the cell increases due to electrolyte consumption, unwanted reactions and formation of further SEI and CEI. The standard deviation of the measurements does not permit any significant conclusions, but there is a tendency that the HFR increases less over the lifetime with larger electrolyte quantities than with cells with small electrolyte quantities.

Conclusions

The investigation on which this paper is based has shown that the energy density as well as the capacity of lithium-ion batteries are

dependent on the electrolyte quantity. Too little electrolyte leads to a loss of capacity and lifetime, whereas too much electrolyte reduces the energy density. For optimal wetting of the cell components with electrolyte, a minimum amount of electrolyte corresponding to the pore volume was identified. Furthermore, the excess of VC was compared to the lack of electrolyte over the lifetime of the cells. Both failure mechanisms can be recognized by different discharge voltages over the capacity. If there is a lack of electrolyte, the voltage drops sharply already at the beginning of the discharging process, whereas a VC excess leads to a later, but stronger drop of the voltage at the end of the discharging phase. The CV-share over cycling increases with decreasing electrolyte quantity and without influence of excessive VC quantities. Therefore, it is assumed that without excessive additive VC and with increasing amount of electrolyte the performance increases over the lifetime, especially at higher C-rates. It was also shown that the HFR decreases with increasing quantity of electrolyte. For an electrolyte quantity which is too low, EIS can be used to detect the redistribution of the electrolyte within the pores. Thus, EIS cannot only be used to measure the electolyte distribution after the wetting of cell components has been completed, but also helps to find out whether a sufficient amount of electrolyte has been dosed for the given pore structure. The production steps after filling and cycling have an influence on the internal resistance of the cell as a function of the dosed electrolyte volume, which can also be measured by EIS and observed by HFR.

Not only the need of adapting the composition of the electrolyte to the active materials and the amount of electrolyte per surface of the active material does become clear, but also the need of adapting the amount of electrolyte to the application desired by the customer.

Acknowledgments

The authors are gratefully indebted to the German Federal Ministry of Education and Research (BMBF) for funding their research within the project Cell-Fi (grant number 03XP0069C). The authors thank Tanja Zünd for her critical feedback on the electrochemical interpretation, Jan Bernd Habedank and Hoda Mohseni for technical support in laser cutting and ultrasonic welding as well as Gamry Instruments for the loan of the potentiostat.

ORCID

Florian J. Günter https://orcid.org/0000-0002-5967-6801

References

1. R. Schmuch, R. Wagner, G. Hörpel, T. Placke, and M. Winter, Performance and cost of materials for lithium-based rechargeable automotive batteries, *Nature Energy*, **3**(4), 267 (2018).
2. B. Scrosati and J. Garche, Lithium batteries: Status, prospects and future, *Journal of Power Sources*, **195**(9), 2419 (2010).
3. D. Andre, S.-J. Kim, P. Lamp, S. F. Lux, F. Maglia, O. Paschos, and B. Stiaszny, Future generations of cathode materials: An automotive industry perspective, *Journal of Materials Chemistry A*, **3**(13), 6709 (2015).
4. A. Sakti, J. J. Michalek, E. R. Fuchs, and J. F. Whitacre, A techno-economic analysis and optimization of li-ion batteries for light-duty passenger vehicle electrification, *Journal of Power Sources*, **273**, 966 (2015).
5. S. J. An, J. Li, C. Daniel, D. Mohanty, S. Nagpure, and D. L. Wood, The state of understanding of the lithium-ion-battery graphite solid electrolyte interphase (sei) and its relationship to formation cycling, *Carbon*, **105**, 52 (2016).
6. M. Lanz, E. Lehmann, R. Imhof, I. Exnar, and P. Novk, In situ neutron radiography of lithium-ion batteries during charge/discharge cycling, *Journal of Power Sources*, **101**(2), 177 (2001).
7. K. Xu, Electrolytes and interphases in li-ion batteries and beyond, *Chemical reviews*, **114**(23), 11503 (2014).
8. L. Somerville, J. Bareño, S. Trask, P. Jennings, A. McGordon, C. Lyness, and I. Bloom, The effect of charging rate on the graphite electrode of commercial lithium-ion cells: A post-mortem study, *Journal of Power Sources*, **335**, 189 (2016).
9. A. Wang, S. Kadam, H. Li, S. Shi, and Y. Qi, Review on modeling of the anode solid electrolyte interphase (sei) for lithium-ion batteries, *npj Computational Materials*, **4**(1), 359 (2018).
10. T. Knoche and G. Reinhart, Electrolyte filling of large-scale lithium-ion batteries: Main influences and challenges for production technology, *Applied Mechanics and Materials*, **794**, 11 (2015).
11. D. L. Wood, J. Li, and C. Daniel, Prospects for reducing the processing cost of lithium ion batteries, *Journal of Power Sources*, **275**, 234 (2015).
12. A. Kwade, W. Haselrieder, R. Leithoff, A. Modlinger, F. Dietrich, and K. Droeder, Current status and challenges for automotive battery production technologies, *Nature Energy*, **3**(4), 290 (2018).
13. W. J. Weydanz, H. Reisenweber, A. Gottschalk, M. Schulz, T. Knoche, G. Reinhart, M. Masuch, J. Franke, and R. Gilles, Visualization of electrolyte filling process and influence of vacuum during filling for hard case prismatic lithium ion cells by neutron imaging to optimize the production process, *Journal of Power Sources*, **380**, 126 (2018).
14. J. B. Habedank, F. J. Günter, N. Billot, R. Gilles, T. Neuwirth, G. Reinhart, and M. F. Zaeh, Rapid electrolyte wetting of lithium-ion batteries containing laser structured electrodes: in situ visualization by neutron radiography, *The International Journal of Advanced Manufacturing Technology*, **273**, 966 (2019).
15. J. B. Habedank, L. Kraft, A. Rheinfeld, C. Krezdorn, A. Jossen, and M. F. Zaeh, Increasing the discharge rate capability of lithium-ion cells with laser-structured graphite anodes: Modeling and simulation, *Journal of The Electrochemical Society*, **165**(7), A1563 (2018).
16. M.-S. Wu, T.-L. Liao, Y.-Y. Wang, and C.-C. Wan, Assessment of the wettability of porous electrodes for lithium-ion batteries, *Journal of Applied Electrochemistry*, **34**(8), 797 (2004).
17. F. J. Günter, J. B. Habedank, D. Schreiner, T. Neuwirth, R. Gilles, and G. Reinhart, Introduction to electrochemical impedance spectroscopy as a measurement method for the wetting degree of lithium-ion cells, *Journal of The Electrochemical Society*, **165**(14), A3249 (2018).
18. T. Knoche, V. Zinth, M. Schulz, J. Schnell, R. Gilles, and G. Reinhart, In situ visualization of the electrolyte solvent lling process by neutron radiography, *Journal of Power Sources*, **331**, 267 (2016).
19. F. J. Günter, R. Gilles, M. Schulz, S. Rössler, W. Braunwarth, and G. Reinhart, Influence of the Cell Format on the Filling Process of Lithiumion Cells, *Energy Technology* (2019).
20. G. Reinhart, T. Zeilinger, J. Kurfer, M. Westermeier, C. Thiemann, M. Glonegger, M. Wunderer, C. Tammer, M. Schweier, and M. Heinz, Research and demonstration center for the production of large-area lithium-ion cells, in: G. Schuh (Ed.), *Future trends in production engineering*, Springer, Berlin, 2013, pp. 3−12.
21. T. Günther, N. Billot, J. Schuster, J. Schnell, F. B. Spingler, and H. A. Gasteiger, The manufacturing of electrodes: Key process for the future success of lithium-ion batteries, *Advanced Materials Research*, **1140**, 304 (2016).
22. T. Knoche, F. Surek, and G. Reinhart, A process model for the electrolyte filling of lithium-ion batteries, *Procedia CIRP*, **41**, 405 (2016).
23. N. Fries and M. Dreyer, An analytic solution of capillary rise restrained by gravity, *Journal of colloid and interface science*, **320**(1), 259 (2008).
24. X.-G. Yang, Y. Leng, G. Zhang, S. Ge, and C.-Y. Wang, Modeling of lithium plating induced aging of lithium-ion batteries: Transition from linear to nonlinear aging, *Journal of Power Sources*, **360**, 28 (2017).
25. K. G. Gallagher, S. E. Trask, C. Bauer, T. Woehrle, S. F. Lux, M. Tschech, P. Lamp, B. J. Polzin, S. Ha, B. Long, Q. Wu, W. Lu, D. W. Dees, and A. N. Jansen, Optimizing areal capacities through understanding the limitations of lithium-ion electrodes, *Journal of The Electrochemical Society*, **163**(2), A138 (2016).
26. Y. Qian, C. Schultz, P. Niehoff, T. Schwieters, S. Nowak, F. M. Schappacher, and M. Winter, Investigations on the electrochemical decomposition of the electrolyte additive vinylene carbonate in li metal half cells and lithium ion full cells, *Journal of Power Sources*, **332**, 60 (2016).
27. S. F. Schuster, T. Bach, E. Fleder, J. Müller, M. Brand, G. Sextl, and A. Jossen, Nonlinear aging characteristics of lithium-ion cells under different operational conditions, *Journal of Energy Storage*, **1**, 44 (2015).
28. Q. Liu, C. Du, B. Shen, P. Zuo, X. Cheng, Y. Ma, G. Yin, and Y. Gao, Understanding undesirable anode lithium plating issues in lithium-ion batteries, *RSC Advances*, **6**(91), 88683 (2016).
29. M. Klett, R. Eriksson, J. Groot, P. Svens, K. Ciosek Högström, R. W. indström, H. Berg, T. Gustafson, G. Lindbergh, and K. Edström, Non-uniform aging of cycled commercial lifepo4//graphite cylindrical cells revealed by post-mortem analysis, *Journal of Power Sources*, **257**, 126 (2014).
30. S. S. Zhang, The effect of the charging protocol on the cycle life of a li-ion battery, *Journal of Power Sources*, **161**(2), 1385 (2006).
31. V. Agubra and J. Fergus, Lithium ion battery anode aging mechanisms, *Materials (Basel, Switzerland)*, **6**(4), 1310 (2013).